Inorg. Chem. **2008**, *47*, 4918−4929

Trinuclear Heterobimetallic Ni_2Ln complexes $[L_2Ni_2Ln][ClO_4]$ (Ln = La, Ce, Pr, Nd, Sm, Eu, Gd, Tb, Dy, Ho, and Er; LH_3 = (S)P[N(Me)N=CH−C_6H_3-*2*-OH-*3*-OMe]$_3$): From Simple Paramagnetic Complexes to Single-Molecule Magnet Behavior

Vadapalli Chandrasekhar,*,† Balasubramanian Murugesa Pandian,† Ramamoorthy Boomishankar,‡ Alexander Steiner,‡ Jagadese J. Vittal,§ Ahmad Houri,|| and Rodolphe Clérac*,||

Department of Chemistry, Indian Institute of Technology Kanpur, Kanpur-208 016, India, Department of Chemistry, University of Liverpool, Liverpool-L69 7ZD, U.K. Department of Chemistry, National University of Singapore, Singapore, Université Bordeaux 1; CNRS, Centre de Recherche Paul Pascal - UPR8641, 115 avenue du Dr. Albert Schweitzer, 33600 Pessac, France

Received January 31, 2008

The reaction of LH_3 with $Ni(ClO_4)_2 \cdot 6H_2O$ and lanthanide salts in a 2:2:1 ratio in the presence of triethylamine leads to the formation of the trinuclear complexes $[L_2Ni_2Ln][ClO_4]$ (Ln = La (**2**), Ce (**3**), Pr (**4**), Nd (**5**), Sm (**6**), Eu (**7**), Gd (**8**), Tb (**9**), Dy (**10**), Ho (**11**) and Er (**12**) and L: (S)P[N(Me)N=CH−C_6H_3-*2*-O-*3*-OMe]$_3$). The cationic portion of these complexes consists of three metal ions that are arranged in a linear manner. The two terminal nickel(II) ions are coordinated by imino and phenolate oxygen atoms (3N, 3O), whereas the central lanthanide ion is bound to the phenolate and methoxy oxygen atoms (12O). The Ni−Ni separations in these complexes range from 6.84 to 6.48 Å. The Ni−Ni, Ni−Ln and Ln−$O_{phenolate}$ bond distances in **2**−**12** show a gradual reduction proceeding from **2** to **12** in accordance with lanthanide contraction. Whereas all of the compounds (**2**−**12**) are paramagnetic systems, **8** displays a remarkable $S_T = {}^{11}/_2$ ground state induced by an intramolecular Ni· · ·Gd ferromagnetic interaction, and **10** is a new mixed metal 3d/4f single-molecule magnet generated by the high-spin ground state of the complex and the magnetic anisotropy brought by the dysprosium(III) metal ion.

Introduction

There is considerable research interest in recent years on the study of new molecular magnetic materials.[1–7] This interest, although largely influenced by the prospect of discovering new technological applications,[8] is also driven by more fundamental interest including efforts to understand magnetic behavior of the widest diversity (ranging from paramagnetism to superparamagnetism and single-molecule magnet (SMM) properties) among transition-metal complexes.[9–12] Although most of the emphasis has been on polynuclear metal complexes[9–12] spurred undoubtedly by the SMM behavior of the dodecanuclear manganese cluster $[Mn_{12}O_{12}(CH_3COO)_{16}(H_2O)_4]$,[13] there have also been many recent reports of relatively low-nuclearity complexes.[14] These

* To whom correspondence should be addressed. Fax: (+91)-512-2597436; E-mail: vc@iitk.ac.in (V.C.), clerac@crpp-bordeaux.cnrs.fr (R.C.).
† Indian Institute of Technology Kanpur.
‡ University of Liverpool.
§ National University of Singapore.
|| CNRS.

(1) Gatteschi, D.; Sessoli, R. Villain, J. *Molecular Nanomagnets*, Oxford University Press: Oxford, 2006.
(2) (a) Kahn, O. *Struct. Bonding (Berlin)* **1987**, *68*, 89. (b) Kahn, O. *Acc. Chem. Res.* **2000**, *33*, 647.
(3) Ôkawa, H.; Furutachi, H.; Fenton, D. E. *Coord. Chem. Rev.* **1998**, *174*, 51.
(4) Winpenny, R. E. P. *Chem. Soc. Rev.* **1998**, *27*, 447.
(5) Sakamoto, M.; Manseki, K.; Ôkawa, H. *Coord. Chem. Rev.* **2001**, *379*, 219–221.
(6) Benelli, C.; Gatteschi, D. *Chem. Rev.* **2002**, *102*, 2369.
(7) (a) Christou, G.; Gatteschi, D.; Hendrickson, D. N.; Sessoli, R. *MRS Bull.* **2000**, *25*, 66. (b) Gatteschi, D.; Sessoli, R. *Angew. Chem., Int. Ed.* **2003**, *42*, 268. (c) Miyasaka, H.; Clérac, R. *Bull. Chem. Soc. Jpn.* **2005**, *78*, 1725.
(8) Ritter, S. K. *Chem. Eng. News* **2004**, *82*, 29.
(9) (a) Friedman, J. R.; Sarachik, M. P.; Tejada, J.; Ziolo, R. *Phys. Rev. Lett.* **1996**, *76*, 3830. (b) Wernsdorfer, W.; Sessoli, R. *Science* **1999**, *284*, 133. (c) Wernsdorfer, W.; Soler, M.; Christou, G.; Hendrickson, D. N *J. Appl. Phys.* **2002**, *91*, 7164. (d) Wernsdorfer, W.; Chakov, N. E.; Christou, G *Phys. Rev. Lett.* **2005**, *9* (1−4), 037203.

10.1021/ic800199x CCC: $40.75
Published on Web 05/07/2008

include mixed 3d/4f metal aggregates,[15,16] some of which have been shown to possess SMM behavior.[16] It may also be pointed out that some mononuclear 4f metal complexes have been shown to possess interesting magnetic behavior.[17]

Recently, we have designed a new phosphorus-supported ligand, LH_3, which has been shown to effectively bind two Co(II) and one Gd(III) ions in a linear Co−Gd−Co array, $[L_2Co_2Gd][NO_3]$. This latter complex has been shown to be a novel single-molecule magnet.[18] This result has encouraged us to explore the utility of LH_3 for preparing other 3d/4f metal aggregates. Recent reports[19] on Ni^{II}/4f compounds prompted us to examine a nearly full range of Ni_2Ln compounds. Such complete studies, while relatively less known in literature, allow an examination of the structural and magnetic properties of Ni^{II}/4f complexes as the 4f metal ion is changed. Accordingly, herein we report the synthesis, structural characterization, and magnetism of a $[L_2Ni_2Ln][ClO_4]$ family of compounds (Ln = La (**2**), Ce (**3**), Pr (**4**), Nd (**5**), Sm (**6**), Eu (**7**), Gd (**8**), Tb (**9**), Dy (**10**), Ho (**11**), and Er (**12**) and L: (S)P[N(Me)N=CH−C_6H_3-*2*-O-*3*-OMe]$_3$).

Experimental section

Reagents and General Procedures. Solvents and other general reagents used in this work were purified according to standard procedures.[20] $P(S)Cl_3$ and 3-methoxy salicylaldehyde (Fluka, Switzerland) were used as purchased. *N*-Methylhydrazine was obtained as a gift from the Vikram Sarabhai Space Research Centre, Thiruvananthapuram, India, and used as received. LH_3 (**1**) was synthesized by a procedure as reported earlier.[18] $Ni(ClO_4)_2 \cdot 6H_2O$ was prepared by the dissolution of nickel carbonates in perchloric acids. $Ln(X)_3 \cdot nH_2O$ (X = NO_3 for **2**−**6**, **8**−**10**, and **12**; X = Cl for **7** and **11**) were obtained from Aldrich Chemical Co. and used as such.

Preparation of Trinuclear Metal 2−12. A general procedure was applied for the preparation of these metal complexes. The ligand LH_3 (0.20 g, 0.333 mmol) was solubilized in a mixture of chloroform (30 mL) and methanol (30 mL). $Ni(ClO_4)_2 \cdot 6H_2O$ (0.12

(10) (a) Benelli, C.; Cano, J.; Journaux, Y.; Sessoli, R.; Solan, G. A.; Winpenny, R. E. P. *Inorg. Chem.* **2001**, *40*, 188. (b) Brechin, E. K.; Boskovic, C.; Wernsdorfer, W.; Yoo, J.; Yamaguchi, A.; Sanudo, E. C.; Concolino, T. R.; Rheingold, A. L.; Ishimoto, H.; Hendrickson, D. N.; Christou, G. *J. Am. Chem. Soc.* **2002**, *124*, 9710. (c) Koizumi, S.; Nihei, M.; Nakano, M.; Oshio, H. *Inorg. Chem.* **2005**, *44*, 1208. (d) Li, D.; Parkin, S.; Wang, G.; Yee, G. T.; Prosvirin, A. V.; Holmes, S. M. *Inorg. Chem.* **2005**, *44*, 4903. (e) Stamatatos, T. C.; Foguet-Albiol, D.; Stoumpos, C. C.; Raptopoulou, C. P.; Terzis, A.; Wernsdorfer, W.; Perlepes, S. P.; Christou, G. *J. Am. Chem. Soc.* **2005**, *127*, 15380. (f) Li, D.; Clérac, R.; Parkin, S.; Wang, G.; Yee, G. T.; Holmes, S. M. *Inorg. Chem.* **2006**, *45*, 5251. (g) Milios, C. J.; Vinslava, A.; Wernsdorfer, W.; Moggach, S.; Parsons, S.; Perlepes, S. P.; Christou, G.; Brechin, E. K. *J. Am. Chem. Soc.* **2007**, *129*, 2754. (h) Yang, C.-I.; Wernsdorfer, W.; Lee, G.-H.; Tsai, H.-L. *J. Am. Chem. Soc.* **2007**, *129*, 456.

(11) (a) Sun, Z.; Grant, C. M.; Castro, S. L.; Hendrickson, D. N.; Christou, G. *Chem. Commun.* **1998**, 721. (b) Oshio, H.; Hoshino, N.; Ito, T. *J. Am. Chem. Soc.* **2000**, *122*, 12602. (c) Murrie, M.; Stöeckli-Evans, H.; Güdel, H. U. *Angew. Chem., Int. Ed.* **2001**, *40*, 1957. (d) Andres, H.; Basler, R.; Blake, A. J.; Cadiou, C.; Chaboussant, G.; Grant, C. M.; Güdel, H.-U.; Murrie, M.; Parsons, S.; Paulsen, C.; Semadini, F.; Villar, V.; Wernsdorfer, W.; Winpenny, R. E. P. *Chem.—Eur. J.* **2002**, *8*, 4867. (e) Dendrinou-Samara, C.; Alexiou, M.; Zaleski, C. M.; Kampf, J. W.; Kirk, M. L.; Kessissoglou, D. P.; Pecoraro, V. L. *Angew. Chem., Int. Ed.* **2003**, *42*, 3763. (f) Schelter, E. J.; Prosvirin, A. V.; Dunbar, K. R. *J. Am. Chem. Soc.* **2004**, *126*, 15004. (g) Langley, S. J.; Helliwell, M.; Sessoli, R.; Rosa, P.; Wernsdorfer, W.; Winpenny, R. E. P. *Chem. Commun.* **2005**, 5029. (h) Biswas, B.; Khanra, S.; Weyhermüller, T.; Chaudhuri, P. *Chem. Commun.* **2007**, 1059.

(12) (a) Winpenny, R. E. P. *J. Chem. Soc., Dalton Trans.* **2002**, 1. (b) Boudalis, A. K.; Donnadieu, B.; Nastopoulos, V.; Clemente-Juan, J. M.; Mari, A.; Sanakis, Y.; Tuchagues, J.-P.; Perlepes, S. P. *Angew. Chem., Int. Ed.* **2004**, *43*, 2266. (c) Oshio, H.; Nihei, M.; Koizumi, S.; Shiga, T.; Nojiri, H.; Nakano, M.; Shirakawa, N.; Akatsu, M. *J. Am. Chem. Soc.* **2005**, *127*, 4568. (d) Li, D.; Parkin, S.; Wang, G.; Yee, G. T.; Clérac, R.; Wernsdorfer, W.; Holmes, S. M. *J. Am. Chem. Soc.* **2006**, *128*, 4214. (e) Kachi-Terajima, C.; Miyasaka, H.; Sugiura, K.-i.; Clérac, R.; Nojiri, H *Inorg. Chem.* **2006**, *45*, 4381. (f) Boudalis, A. K.; Raptopoulou, C. P.; Abarca, B.; Ballesteros, R.; Chadlaoui, M.; Tuchagues, J.-P.; Terzis, A. *Angew. Chem., Int. Ed.* **2006**, *45*, 432.

(13) (a) Lis, T. *Acta Crystallogr.* **1980**, *B36*, 2042. (b) Sessoli, R.; Tsai, H.-L.; Schake, A. R.; Wang, S.; Vincent, J. B.; Folting, K.; Gatteschi, D.; Christou, G.; Hendrickson, D. N *J. Am. Chem. Soc.* **1993**, *115*, 1804. (c) Sessoli, R.; Gatteschi, D.; Caneschi, A.; Novak, M. A. *Nature* **1993**, *365*, 141.

(14) (a) Wittick, L. M.; Murray, K. S.; Moubaraki, B.; Batten, S. R.; Spiccia, L.; Berry, K. J. *Dalton Trans.* **2004**, 1003. (b) Miyasaka, H.; Clérac, R.; Wernsdorfer, W.; Lecren, L.; Bonhomme, C.; Sugiura, K.; Yamashita, M. *Angew. Chem., Int. Ed.* **2004**, *43*, 2801. (c) Scott, R. T. W.; Parsons, S.; Murugesu, M.; Wernsdorfer, W.; Christou, G.; Brechin, E. K. *Chem. Commun.* **2005**, 2083. (d) Accorsi, S.; Barra, A.-L.; Caneschi, A.; Chastanet, G.; Cornia, A.; Fabretti, A. C.; Gatteschi, D.; Mortalo, C.; Olivieri, E.; Parenti, F.; Rosa, P.; Sessoli, R.; Sorace, L.; Wernsdorfer, W.; Zobbi, L. *J. Am. Chem. Soc.* **2006**, *128*, 4742.

(15) (a) Zhang, J.-J.; Hu, S.-M.; Xiang, S.-C.; Sheng, T.; Wu, X.-T.; Li, Y.-M. *Inorg. Chem.* **2006**, *45*, 7173. (b) Wu, G.; Hewitt, I. J.; Mameri, S.; Lan, Y.; Clérac, R.; Anson, C. E.; Qiu, S.; Powell, A. K. *Inorg. Chem.* **2007**, *46*, 7229. (c) Ako, A. M; Mereacre, V.; Clérac, R.; Hewitt, I. J.; Lan, Y.; Anson, C. E.; Powell, A. K *Dalton Trans.* **2007**, 5245. (d) Alley, K. G.; Mukherjee, A.; Clérac, R.; Boskovic, C. *Dalton Trans.* **2008**, 59.

(16) (a) Zaleski, C. M.; Depperman, E. C.; Kampf, J. W.; Kirk, M. L.; Pecoraro, V. L. *Angew. Chem., Int. Ed.* **2004**, *43*, 3912. (b) Osa, S.; Kido, T.; Matsumoto, N.; Re, N.; Pochaba, A.; Mrozinski, J. *J. Am. Chem. Soc.* **2004**, *126*, 420. (c) Mishra, A.; Wernsdorfer, W.; Abboud, K. A.; Christou, G. *J. Am. Chem. Soc.* **2004**, *126*, 15648. (d) He, F.; Tong, M.-L.; Chen, X.-M. *Inorg. Chem.* **2005**, *44*, 8285. (e) Mishra, A.; Wernsdorfer, W.; Parsons, S.; Christou, G.; Brechin, E. K. *Chem. Commun.* **2005**, 2086. (f) Costes, J.-P.; Dahan, F.; Wernsdorfer, W. *Inorg. Chem.* **2006**, *45*, 5. (g) Costes, J.-P.; Auchel, M.; Dahan, F.; Peyrou, V.; Shova, M.; Wernsdorfer, W *Inorg. Chem.* **2006**, *45*, 1924. (h) Mori, F.; Nyui, T.; Ishida, T.; Nogami, T.; Choi, K.-Y.; Nojiri, H. *J. Am. Chem. Soc.* **2006**, *128*, 1440. (i) Aronica, C.; Pilet, G.; Chastanet, G.; Wernsdorfer, W.; Jacquot, J.-F.; Luneau, D. *Angew. Chem., Int. Ed.* **2006**, *45*, 4659. (j) Ferbinteanu, M.; Kajiwara, T.; Choi, K.-Y.; Nojiri, H.; Nakamoto, A.; Kojima, N.; Cimpoesu, F.; Fujimura, Y.; Takaishi, S.; Yamashita, M. *J. Am. Chem. Soc.* **2006**, *128*, 9008. (k) Murugesu, M.; Mishra, A.; Wernsdorfer, W.; Abboud, K. A.; Christou, G. *Polyhedron* **2006**, *25*, 613. (l) Pointillart, F.; Bernot, K.; Sessoli, R.; Gatteschi, D. *Chem.—Eur. J.* **2007**, *13*, 1602. (m) Mereacre, V. M.; Ako, A. M.; Clérac, R.; Wernsdorfer, W.; Filoti, G.; Bartolome, J.; Anson, C. E.; Powell, A. K. *J. Am. Chem. Soc.* **2007**, *129*, 9248. (n) Zaleski, C. M.; Kampf, J. W.; Mallah, T.; Kirk, M. L.; Pecoraro, V. L *Inorg. Chem.* **2007**, *46*, 1954. (o) Hamamatsu, T.; Yabe, K.; Towatari, M.; Osa, S.; Matsumoto, N.; Re, N.; Pochaba, A.; Mrozinski, J.; Gallani, J.-L.; Barla, A.; Imperia, P.; Paulsen, C.; Kappler, J.-P. *Inorg. Chem.* **2007**, *46*, 4458.

(17) (a) Ishikawa, N.; Sugita, M.; Ishikawa, T.; Koshihara, S.; Kaizu, Y *J. Am. Chem. Soc.* **2003**, *125*, 8694. (b) Ishikawa, N.; Sugita, M.; Ishikawa, T.; Koshihara, S.; Kaizu, Y *J. Phys. Chem. B* **2004**, *108*, 11265. (c) Ishikawa, N.; Sugita, M.; Wernsdorfer, W. *J. Am. Chem. Soc.* **2005**, *127*, 3650. (d) Sugita, M.; Ishikawa, N.; Ishikawa, T.; Koshihara, S.; Kaizu, Y *Inorg. Chem.* **2006**, *45*, 1299.

(18) Chandrasekhar, V.; Pandian, B. M.; Azhakar, R.; Vittal, J. J.; Clérac, R. *Inorg. Chem.* **2007**, *46*, 5140.

(19) (a) Xu, Z.; Read, P. W.; Hibbs, D. E.; Hursthouse, M. B.; Abdul Malik, K. M.; Patrick, B. O.; Rettig, S. J.; Seid, M.; Summers, D. A.; Pink, M.; Thompson, R. C.; Orvig, C. *Inorg. Chem.* **2000**, *39*, 508. (b) Bayly, S. R.; Xu, Z.; Patrick, B. O.; Rettig, S. J.; Pink, M.; Thompson, R. C.; Orvig, C. *Inorg. Chem.* **2003**, *42*, 1576. (c) Koner, R.; Lin, H.-H.; Wei, H.-H.; Mohanta, S. *Inorg. Chem.* **2005**, *44*, 3524. (d) Shiga, T.; Ito, N.; Hidaka, A.; Okawa, H.; Kitagawa, S.; Ohba, M. *Inorg. Chem.* **2007**, *46*, 3492.

(20) Furniss, B. S.; Hannaford, A. J.; Smith, P. W. G.; Tatchell, A. R. *Vogel's Text book of Practical Organic Chemistry*, 5th ed., ELBS, Longman: London, 1989.

g, 0.333 mmol) and $Ln(NO_3)_3 \cdot nH_2O$ (0.167 mmol) (for the preparation of **2**−**6**, **8**−**10**, and **12**) and triethylamine (0.4 mL) were added to the chloroform/methanol solution of the ligand, and the reaction mixture was stirred for 12 h to afford a clear solution. This was filtered and the filtrate was evaporated to dryness. The residue obtained was then washed with *n*-hexane and dried. For the preparation of **7** and **10**, $LnCl_3 \cdot nH_2O$ was used as the lanthanide precursor. Triethylamine was used to scavenge the liberated hydrogen chloride. All of the complexes were purified by crystallization. The characterization data for these complexes is given below.

[{(S)P[N(Me)N=CH−C_6H_3-*2*-O-*3*-OMe]$_3$}$_2$$Ni_2$La]$ClO_4 \cdot 2CHCl_3 \cdot 4H_2O$ (2). Yield: 0.236 g, 75.5%. Mp: >295 °C. UV−vis (CH_3CN) λ_{max}, nm (ϵ, M^{-1} cm^{-1}): 576 (76), 799 (49), 993 (74). FTIR ν/cm^{-1}: 1605 (*C*=N), 1088 and 626 (ClO_4). ESI-MS: *m*/*z* 1449$(M)^+$. Anal. Calcd for $C_{56}H_{70}Cl_7LaN_{12}Ni_2O_{20}P_2S_2$: C, 36.21; H, 3.80; N, 9.05; S, 3.45 Found: C, 36.02; H, 3.69; N, 9.12; S, 3.40.

[{(S)P[N(Me)N=CH−C_6H_3-*2*-O-*3*-OMe]$_3$}$_2$$Ni_2$Ce]$ClO_4 \cdot 2CHCl_3 \cdot 4H_2O$ (3). Yield: 0.240 g, 77.6%. Mp: >295 °C. UV−vis (CH_3CN) λ_{max}, nm (ϵ, M^{-1} cm^{-1}): 577 (29), 807 (15), 993 (53). FTIR ν/cm^{-1}: 1603 (*C*=N), 1077 and 619 (ClO_4). ESI-MS: *m*/*z* 1452$(M)^+$. Anal. Calcd for $C_{56}H_{70}CeCl_7N_{12}Ni_2O_{20}P_2S_2$: C, 36.10; H, 3.79; N, 9.02; S, 3.44 Found: C, 36.02; H, 3.69; N, 9.12; S, 3.40.

[{(S)P[N(Me)N=CH−C_6H_3-*2*-O-*3*-OMe]$_3$}$_2$$Ni_2$Pr]$ClO_4 \cdot 2CHCl_3 \cdot 4H_2O$ (4). Yield: 0.220 g, 70.9%. Mp: >295 °C. UV−vis (CH_3CN) λ_{max}, nm (ϵ, M^{-1} cm^{-1}): 579 (25), 810 (14), 993 (51). FTIR ν/cm^{-1}: 1602 (*C*=N), 1077 and 619 (ClO_4). ESI-MS: *m*/*z* 1451$(M)^+$. Anal. Calcd for $C_{56}H_{70}Cl_7N_{12}$ $Ni_2O_{20}P_2PrS_2$: C, 36.17; H, 3.80; N, 9.04; S, 3.44 Found: C, 36.02; H, 3.69; N, 9.12; S, 3.40.

[{(S)P[N(Me)N=CH−C_6H_3-*2*-O-*3*-OMe]$_3$}$_2$$Ni_2$Nd]$ClO_4 \cdot 2CHCl_3 \cdot 4H_2O$ (5). Yield: 0.235 g, 75.6%. Mp: >295 °C. UV−vis (CH_3CN) λ_{max}, nm (ϵ, M^{-1} cm^{-1}): 577 (41), 810 (21), 993 (62). FTIR ν/cm^{-1}: 1602 (*C*=N), 1077 and 620 (ClO_4). ESI-MS: *m*/*z* 1456$(M)^+$. Anal. Calcd for $C_{56}H_{70}NdCl_7N_{12}Ni_2O_{20}P_2S_2$: C, 36.02; H, 3.78; N, 9.00; S, 3.43. Found: C, 36.08; H, 3.70; N, 8.95; S, 3.38

[{(S)P[N(Me)N=CH−C_6H_3-*2*-O-*3*-OMe]$_3$}$_2$$Ni_2$Sm]$ClO_4 \cdot 2CHCl_3 \cdot 4H_2O$ (6). Yield: 0.229 g, 73.4%. Mp: >295 °C. UV−vis (CH3CN) λmax, nm (ϵ, M^{-1} cm^{-1}): 576 (29), 804 (17), 994 (57). FTIR ν/cm^{-1}: 1602 (*C*=N), 1077 and 620 (ClO_4). ESI-MS: *m*/*z* 1462$(M)^+$. Anal. Calcd for $C_{56}H_{70}Cl_7SmN_{12}Ni_2O_{20}P_2S_2$: C, 35.91; H, 3.77; N, 8.97; S, 3.42. Found: C, 35.84; H, 3.69; N, 8.88; S, 3.49.

[{(S)P[N(Me)N=CH−C_6H_3-*2*-O-*3*-OMe]$_3$}$_2$$Ni_2$Eu]$ClO_4 \cdot 2CHCl_3 \cdot 4H_2O$ (7). Yield: 0.242 g, 77.5%. Mp: >295 °C. UV−vis (CH_3CN) λ_{max}, nm (ϵ, M^{-1} cm^{-1}): 579 (25), 810 (14), 993 (51). FTIR ν/cm^{-1}: 1602 (*C*=N), 1078 and 620 (ClO_4). ESI-MS: *m*/*z* 1463 $(M)^+$. Anal. Calcd for $C_{56}H_{70}Cl_7EuN_{12}Ni_2O_{20}P_2S_2$: C, 35.87; H, 3.76; N, 8.97; S, 3.42. Found: C, 35.80; H, 3.73; N, 8.90; S, 3.45.

[{(S)P[N(Me)N=CH−C_6H_3-*2*-O-*3*-OMe]$_3$}$_2$$Ni_2$Gd]$ClO_4 \cdot 2CHCl_3 \cdot 2CH_3OH \cdot 2H_2O$ (8). Yield: 0.26 g, 81.89%. Mp: >295 °C. UV−vis (CH_3CN) λinf > max, nm (ϵ, M^{-1} cm^{-1}): 572 (92), 803 (55), 993 (83). FTIR ν/cm^{-1}: 1602 (*C*=N), 1078 and 620 (ClO_4). ESI-MS: *m*/*z* 1468$(M)^+$. Anal. Calcd for $C_{58}H_{74}Cl_7GdN_{12}Ni_2$-$O_{20}P_2S_2$: C, 35.15; H, 3.90; N, 8.79; S, 3.34. Found: C, 35.26; H, 3.85; N, 8.81; S, 3.30.

[{(S)P[N(Me)N=CH−C_6H_3-*2*-O-*3*-OMe]$_3$}$_2$$Ni_2$Tb]$ClO_4 \cdot 2CHCl_3 \cdot 6H_2O$ (9). Yield: 0.248 g, 77.7%. Mp: >295 °C. UV−vis (CH_3CN) λ_{max}, nm (ϵ, M^{-1} cm^{-1}): 576 (25), 812 (17), 992 (55). FTIR ν/cm^{-1}: 1601 (*C*=N), 1078 and 620 (ClO_4). ESI-MS: *m*/*z* 1469$(M)^+$. Anal. Calcd for $C_{56}H_{74}Cl_7TbN_{12}Ni_2O_{22}P_2S_2$: C, 35.15; H, 3.90; N, 8.79; S, 3.34. Found: C, 35.10; H, 3.85; N, 8.70; S, 3.32.

[{(S)P[N(Me)N=CH−C_6H_3-*2*-O-*3*-OMe]$_3$}$_2$$Ni_2$Dy]$ClO_4 \cdot 2CHCl_3 \cdot CH_3OH \cdot 2H_2O$ (10). Yield: 0.242 g, 77.3%. Mp: >295 °C. UV−vis (CH_3CN) λ_{max}, nm (ϵ, M^{-1} cm^{-1}): 577 (29), 807 (15), 993 (53). FTIR ν/cm^{-1}: 1602 (*C*=N), 1078 and 621 (ClO_4). ESI-MS: *m*/*z* 1474$(M)^+$. Anal. Calcd for $C_{57}H_{70}Cl_7DyN_{12}Ni_2O_{19}P_2S_2$: C, 36.44; H, 3.76; N, 8.95; S, 3.41. Found: C, 36.46; H, 3.85; N, 8.88; S, 3.39.

[{(S)P[N(Me)N=CH−C_6H_3-*2*-O-*3*-OMe]$_3$}$_2$$Ni_2$Ho]$ClO_4 \cdot 2CHCl_3 \cdot 4H_2O$ (11). Yield: 0.252 g, 80.6%. Mp: >295 °C. UV−vis (CH_3CN) λ_{max}, nm (ϵ, M^{-1} cm^{-1}): 577 (40), 811 (24), 994 (74). FTIR ν/cm^{-1}: 1600 (*C*=N), 1087 and 625 (ClO_4). ESI-MS: *m*/*z* 1475$(M)^+$. Anal. Calcd for $C_{56}H_{70}Cl_7HoN_{12}Ni_2O_{20}P_2S_2$: C, 35.71; H, 3.75; N, 8.93; S, 3.40. Found: C, 35.86; H, 3.80; N, 8.98; S, 3.38.

[{(S)P[N(Me)N=CH−C_6H_3-*2*-O-*3*-OMe]$_3$}$_2$$Ni_2$Er]$ClO_4 \cdot 2CHCl_3 \cdot 5H_2O$ (12). Yield: 0.255 g, 80.3%. Mp: >295 °C. UV−vis (CH_3CN) λ_{max}, nm (ϵ, M^{-1} cm^{-1}): 575 (38), 808 (20), 995 (60). FTIR ν/cm^{-1}: 1600 (*C*=N), 1079 and 622 (ClO_4). ESI-MS: *m*/*z* 1476$(M)^+$. Anal. Calcd for $C_{56}H_{72}Cl_7ErN_{12}Ni_2O_{21}P_2S_2$: C, 35.35; H, 3.82; N, 8.84; S, 3.36. Found: C, 35.46; H, 3.85; N, 8.78; S, 3.34.

Instrumentation. Melting points were measured using a JSGW melting point apparatus and are uncorrected. IR spectra were recorded as KBr pellets on a Bruker Vector 22 FTIR spectrophotometer operating from 400−4000 cm^{-1}. UV−vis spectra were recorded on a PerkinElmer LS UV−vis Lambda 20 spectrometer using CH_3CN as solvent. Elemental analyses of the compounds were obtained using a Thermoquest CE instrument CHNS-O, EA/110 model. ESI-MS spectra were recorded on a Micromass Quattro II triple quadrupole mass spectrometer.

Magnetic Measurements. The magnetic susceptibility measurements were obtained using a Quantum Design SQUID magnetometer MPMS-XL. This magnetometer works between 1.8 and 400 K for dc applied fields ranging from −7 to 7 T. Measurements were performed on finely ground crystalline samples. *M* versus *H* measurements have been performed at 100 K to check for the presence of ferromagnetic impurities. After ascertaining the absence of such impurities, ac susceptibility measurements were performed using an oscillating ac field of 3 Oe and ac frequencies ranging from 1 to 1500 Hz. It is worth noting that an out-of-phase ac signal has been detected only for **10** (vide infra). The magnetic data were corrected for the sample holder and the diamagnetic contribution.

X-ray Crystallography. The crystal data and the cell parameters for **2**−**12** are given in Tables 1–3. Single crystals suitable for X-ray crystallographic analyses were obtained by a slow diffusion of *n*-hexane into a solution of chloroform/methanol mixture of these compounds (**2**−**12**). The crystal data for **2**−**12** have been collected on a Bruker SMART CCD diffractometer using a Mo Kα sealed tube. The program *SMART*[22a] was used for collecting frames of data, indexing reflection, and determining lattice parameters, *SAINT*[22a] for integration of the intensity of reflections and scaling, *SADABS*[22b] for absorption correction, and *SHELXTL*[22c,d] for space group and structure determination and least-squares refinements on F^2. All structures were solved by direct methods using the programs *SHELXS-97*[22e] and refined by full-matrix least-squares methods against F^2 with *SHELXL-97*.[22e] Hydrogen atoms were fixed at

(21) Chandrasekhar, V.; Azhakar, R.; Andavan, G. T. S.; Krishnan, V.; Zacchini, S.; Bickley, J. F.; Steiner, A.; Butcher, R. J.; Kögerler, P. *Inorg. Chem.* **2003**, *42*, 5989.

Table 1. Crystallographic Data and Refinement for **2**−**5**

	2	3	4	5
empirical formula	$C_{56}H_{70}Cl_7LaN_{12}Ni_2O_{20}P_2S_2$	$C_{56}H_{70}Cl_7CeN_{12}Ni_2O_{20}P_2S_2$	$C_{56}H_{70}Cl_7PrN_{12}Ni_2O_{20}P_2S_2$	$C_{56}H_{70}Cl_7NdN_{12}Ni_2O_{20}P_2S_2$
fw	1861.78	1862.99	1863.78	1867.11
T (K)	223(2)	223(2)	100(2)	223(2)
wavelength (Å)	0.71073	0.71073	0.71073	0.71973
cryst syst	monoclinic	monoclinic	monoclinic	monoclinic
space group	$C2$	$C2$	$C2$	$C2$
unit cell dimensions (Å, deg)	a = 20.891(2) b = 11.7396(12) c = 17.9669(18) α = 90 β = 120.281(2) γ = 90	a = 20.841(2) b = 11.7806(11) c = 18.1005(17) α = 90 β = 121.333(2) γ = 90	a = 20.732(4) b = 11.7097(11) c = 18.009(4) α = 90 β = 121.097(5) γ = 90	a = 20.9618(18) b = 11.7588(11) c = 17.9361(16) α = 90 β = 120.633(5) γ = 90
V (Å^3)	3805.2(7)	3795.9(6)	3743.6(12)	3804.0(6)
Z	2	2	2	2
d_{calcd} (g cm^{-3})	1.625	1.630	1.654	1.630
absorption coefficient (mm^{-1})	1.458	1.499	1.563	1.580
F(000)	1888	1890	1892	1894
cryst size (mm^3)	0.30 × 0.25 × 0.17	0.35 × 0.23 × 0.13	0.2 × 0.2 × 0.2	0.4 × 0.3 × 0.2
Θ range (deg)	1.96 to 24.99	1.96 to 29.34	4.17 to 25.02	1.32 to 25.00
limiting indices	$-24 \le h \le 24$, $-13 \le$ k ≤ 10, $-21 \le l \le 21$	$-28 \le h \le 27$, $-15 \le k \le 16$, $-23 \le l \le 22$	$-24 \le h \le 24$, $-13 \le k \le 13$, $-19 \le l \le 21$	$-22 \le h \le 24$, $-13 \le k \le 13$, $-21 \le l \le 14$
reflns collected	11 335	14 314	9700	11 333
independent reflns	5091 [R(int) = 0.0237]	8581 [R(int) = 0.0259]	6303 [R(int) = 0.0385]	6520 [R(int) = 0.0234]
completeness to θ (%)	99.9	91.6	99.0	100.0
refinement method	Full-matrix least-squares on F^2			
data/restraints/params	5091/14/459	8581/7/460	6303/1/484	6520/7/463
GOF on F^2	1.071	1.046	1.024	1.083
Flack parameter	0.54(2)	0.483(15)	0.392(12)	−0.043(13)
final R indices [$I>2\sigma(I)$]	R1 = 0.0435, wR2 = 0.1223	R1 = 0.0502, wR2 = 0.1277	R1 = 0.0385, wR2 = 0.0977	R1 = 0.0425, wR2 = 0.1153
R indices (all data)	R1 = 0.0454, wR2 = 0.1240	R1 = 0.0565, wR2 = 0.1328	R1 = 0.0425, wR2 = 0.0998	R1 = 0.0465, wR2 = 0.1234
largest diff. peak and hole (e•Å^{-3})	1.323 and −0.802	1.580 and −0.713	1.051 and −0.770	0.942 and −0.716

Table 2. Crystallographic Data and Refinement for **6**−**9**

	6	7	8	9
empirical formula	$C_{56}H_{70}Cl_7SmN_{12}Ni_2O_{20}P_2S_2$	$C_{56}H_{70}Cl_7EuN_{12}Ni_2O_{20}P_2S_2$	$C_{58}H_{74}Cl_7GdN_{12}Ni_2O_{20}P_2S_2$	$C_{56}H_{74}Cl_7TbN_{12}Ni_2O_{22}P_2S_2$
fw	1873.22	1874.83	1908.17	1917.82
T (K)	223(2)	223(2)	100(2)	100(2)
wavelength (Å)	0.71073	0.71073	0.71069	0.71073
cryst syst	monoclinic	monoclinic	monoclinic	monoclinic
space group	$C2$	$C2$	$C2$	$C2$
unit cell dimensions (Å, deg)	a = 21.224(2) b = 11.8162(12) c = 17.9516(18) α = 90 β = 120.854(2) γ = 90	a = 21.993(2) b = 11.7696(12) c = 17.8973(18) α = 90 β = 120.896(2) γ = 90	a = 20.8185(5) b = 11.710(5) c = 17.861(5) α = 90 β = 120.900(5) γ = 90	a = 20.8515(13) b = 11.7155(6) c = 17.8249(12) α = 90 β = 120.809(2) γ = 90
V (Å^3)	3864.9(7)	3794.5(7)	3736(2)	3739.9(4)
Z	2	2	2	2
d_{calcd} (g cm^{-3})	1.610	1.641	1.696	1.703
absorption coefficient (mm^{-1})	1.643	1.726	1.802	1.862
F(000)	1898	1900	1934	1944
cryst size (mm^3)	0.4 × 0.12 × 0.1	0.37 × 0.33 × 0.23	0.20 × 0.20 × 0.16	0.20 × 0.20 × 0.15
Θ range (deg)	1.93 to 25.00	1.95 to 25.00	4.08 to 25.02	4.08 to 25.03
limiting indices	$-18 \le h \le 25$, $-14 \le k \le 14$, $-21 \le l \le 20$	$-24 \le h \le 23$, $-13 \le k \le 13$, $-21 \le l \le 20$	$-24 \le h \le 20$, $-12 \le k \le 13$, $-11 \le l \le 21$	$-24 \le h \le 20$, $-13 \le k \le 13$, $-21 \le l \le 21$
reflns collected	11553	11208	9879	9715
independent reflns	6513 [R(int) = 0.0275]	6463 [R(int) = 0.0172]	6193 [R(int) = 0.0226]	6427 [R(int) = 0.0271]
completeness to θ (%)	99.9	99.9	99.2	99.4
refinement method	Full-matrix least-squares on F^2			
data/restraints/params	6513/14/461	6463/7/459	6193/7/477	6427/1/479
GOF on F^2	1.061	1.065	1.016	1.057
Flack parameter	0.338(14)	0.009(10)	0.548(10)	0.375(9)
Final R indices [$I>2\sigma(I)$]	R1 = 0.0473, wR2 = 0.1223	R1 = 0.0371, wR2 = 0.1072	R1 = 0.0361, wR2 = 0.0857	R1 = 0.0388, wR2 = 0.0926
R indices (all data)	R1 = 0.0534, wR2 = 0.1271	R1 = 0.0391, wR2 = 0.1088	R1 = 0.0377, wR2 = 0.0867	R1 = 0.0424, wR2 = 0.0955
largest diff. peak and hole (e•Å^{-3})	0.865 and −0.504	1.167 and −0.594	1.112 and −0.634	1.214 and −0.484

calculated positions, and their positions were refined by a riding model. All non-hydrogen atoms were refined with anisotropic displacement parameters. The disordered water molecules were refined isotropically. The crystals are racemically twinned, showing appreciable Flack parameters. The figures have been generated using *Diamond 3.1e* software.[22f]

Results and Discussion

Synthesis and Structural Characterization. The ligand LH_3 (**1**, Scheme 1) was synthesized by the procedure reported by us earlier and involved the condensation of (S)P[N(Me)NH_2]$_3$ with *o*-vanillin.[18] LH_3 is a multisite coordination ligand and has nine coordination sites in the form of three imino nitrogen atoms, three phenolic oxygen atoms, and three oxygen atoms of the −OMe group. Although the latter are weakly binding toward transition metal ions, their effectiveness in coordination to lanthanide ions has been demonstrated. LH_3 reacts with $Ni(ClO_4)_2 \cdot 6H_2O$ and $LnX_3 \cdot nH_2O$ in a 2:2:1 stoichiometric ratio in the presence of triethylamine

Table 3. Crystallographic Data and Refinement for **10**−**12**

	10	11	12
empirical formula	$C_{57}H_{70}Cl_7DyN_{12}Ni_2O_{19}P_2S_2$	$C_{56}H_{70}Cl_7HoN_{12}Ni_2O_{20}P_2S_2$	$C_{56}H_{72}Cl_7ErN_{12}Ni_2O_{21}P_2S_2$
fw	1881.38	1887.80	1908.15
T (K)	110(2)	223(2)	100(2)
wavelength (Å)	0.71073	0.71073	0.71073
cryst syst	monoclinic	monoclinic	monoclinic
space group	$C2$	$C2$	$C2$
unit cell dimensions (Å, deg)	$a = 20.8539(13)$	$a = 21.055(3)$	$a = 20.8840(18)$
	$b = 11.7507(6)$	$b = 11.7993(13)$	$b = 11.7482(8)$
	$c = 17.8638(12)$	$c = 17.816(2)$	$c = 17.7621(16)$
	$\alpha = 90$	$\alpha = 90$	$\alpha = 90$
	$\beta = 121.267(2)$	$\beta = 121.178(3)$	$\beta = 121.083(2)$
	$\gamma = 90$	$\gamma = 90$	$\gamma = 90$
V (Å^3)	3741.7(4)	3786.7(8)	3732.2(5)
Z	2	2	2
d_{calcd} (g cm^{-3})	1.67	1.656	1.698
absorption coefficient (mm^{-1})	1.91	1.946	2.040
F(000)	1902	1908	3860
cryst size (mm^3)	0.3 × 0.3 × 0.3	0.23 × 0.2 × 0.18	0.2 × 0.2 × 0.2
Θ range (deg)	4.15 to 25.03	1.34 to 29.46	4.08 to 25.02
limiting indices	$-24 \le h \le 20$, $-13 \le k \le 13$, $-21 \le l \le 21$	$-18 \le h \le 28$, $-15 \le k \le 16$, $-23 \le l \le 13$	$-24 \le h \le 19$, $-11 \le k \le 13$, $-20 \le l \le 21$
reflns collected	9856	14371	9706
independent reflns	6437 [R(int) = 0.0178]	9178 [R(int) = 0.0248]	5208 [R)int) = 0.0229]
completeness to θ (%)	99.3	91.4	98.8
refinement method	Full-matrix least-squares on F^2		
data/restraints/params	6437/1/473	9178/7/464	5208/20/470
GOF on F^2	1.052	1.059	1.045
Flack parameter	0.419(8)	0.353(8)	0.536(8)
Final R indices [$I>2\sigma(I)$]	R1 = 0.0327, wR2 = 0.0870	R1 = 0.0447, wR2 = 0.1157	R1 = 0.0303, wR2 = 0.0800
R indices (all data)	R1 = 0.0338, wR2 = 0.0877	R1 = 0.0496, wR2 = 0.1220	R1 = 0.0316, wR2 = 0.0806
largest diff. peak and hole (e·Å^{-3})	1.172 and −0.517	1.638 and −0.651	1.103 and −0.558

Scheme 1

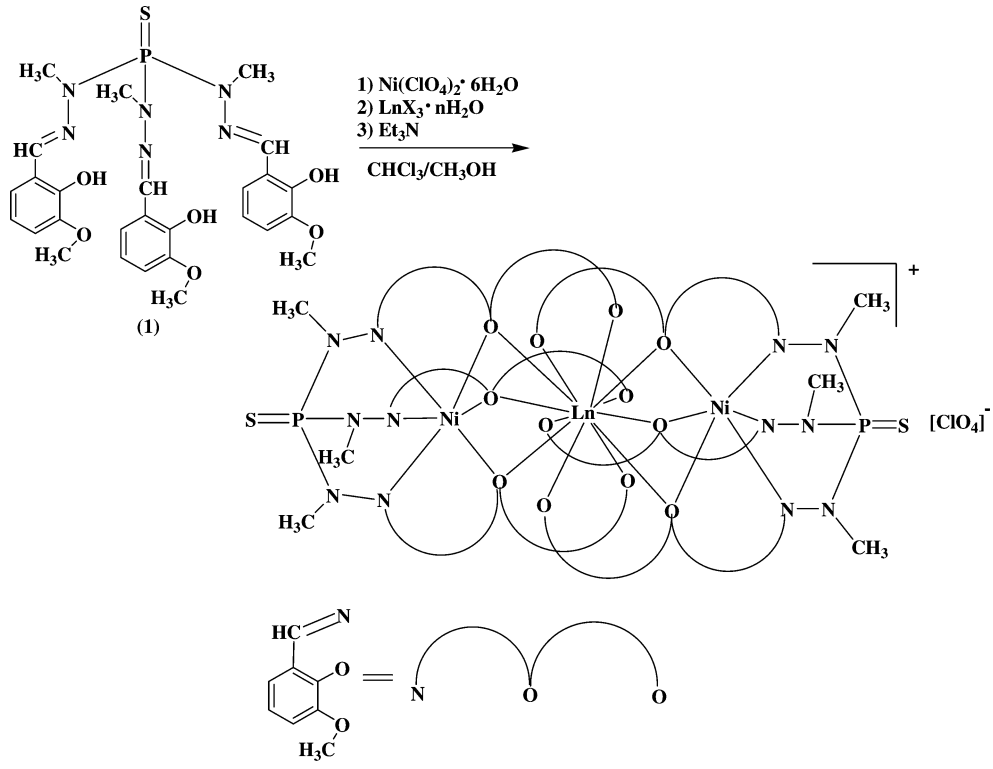

Ln = La (2); Ce (3); Pr (4); Nd (5); Sm (6) Eu (7); Gd (8); Tb (9); Dy (10); Ho (11) and Er (12)
X = Cl (7 & 11) ; X = NO_3 (2-6, 8-10 & 12)

to afford the heterometallic trinuclear **2**−**12** in excellent yields (≥75%, Experimental section) (Scheme 1). **2**−**12** retain their trinuclear structures also in solution as evidenced by the detection of their molecular ion peaks in their ESI-MS spectra (Experimental section). UV−vis spectra were recorded for all of the compounds in CH_3CN. In the visible

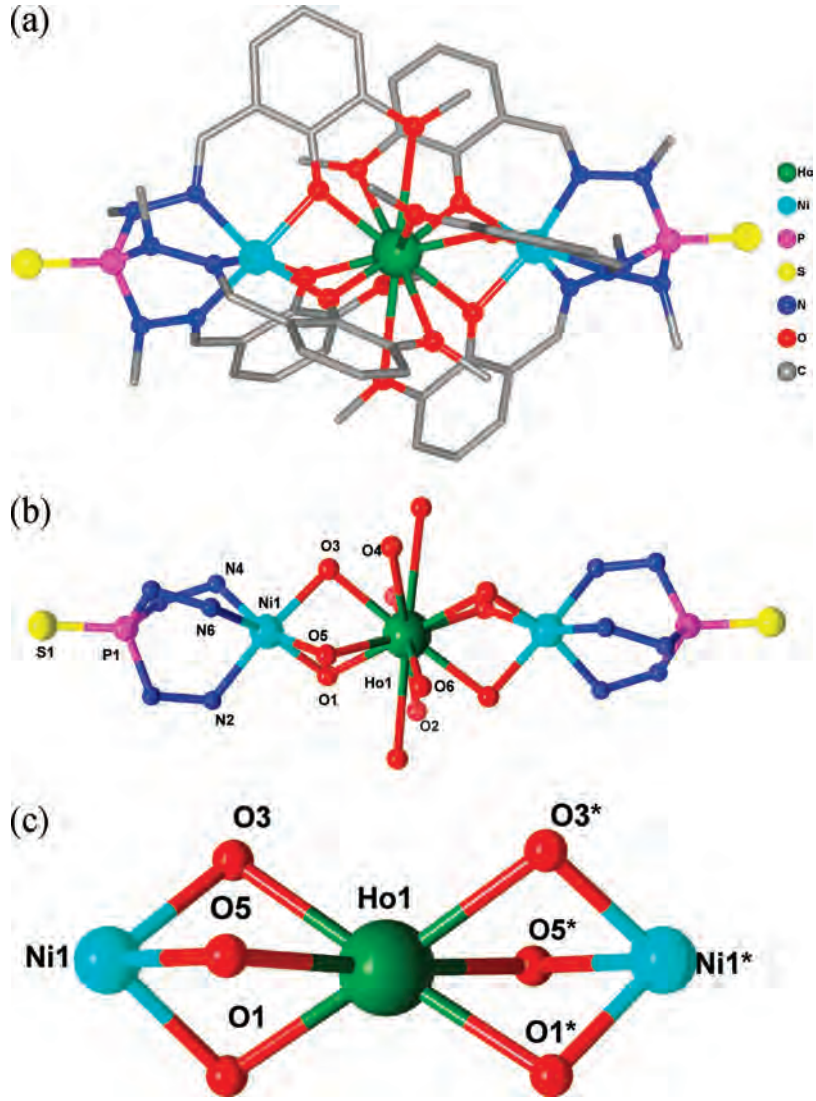

Figure 1. (a) Cationic part of the compound $[L_2Ni_2Ho]^+$ (**11**); hydrogen atoms, perchlorate anions, and solvent molecules omitted for clarity. (b) Coordination environment of nickel and holmium in $[L_2Ni_2Ho]^+$ (**11**); carbon and hydrogen atoms, perchlorate anions, and solvent molecules omitted for clarity. (c) View of the Ni−Ho−Ni core with its intermetal ion bridges realized by the phenolate oxygen atoms; other atoms are omitted for clarity.

region, all of the complexes show two absorption peaks around 580 and 990 nm and one shoulder around 810 nm. The first two peaks are assigned due to $^3A_{2g} \rightarrow {}^3T_{2g}$ and $^3A_{2g} \rightarrow {}^3T_{1g}$ transitions and the 810 nm shoulder to the $^3A_{2g} \rightarrow {}^1E_g$ transition.[19] The similarity of the optical spectrum for all of the complexes is indicative of the invariance of the coordination environment around nickel(II) centers in these complexes.

The molecular structures of **2**−**12** were confirmed by their single-crystal X-ray diffraction analysis. **2**−**12** crystallized in the monoclinic *C*2 space group. The asymmetric unit of these crystal structures contains only half of a molecule. The X-ray crystallographic analysis reveals that **2**−**12** possess similar molecular structure and contain a heterobimetallic cation $[L_2Ni_2Ln]^+$ and one counter perchlorate anion to balance the charge. As a representative example, the structure of the $[L_2Ni_2Ho]^+$ cationic portion of **11** is shown in Figure 1. The molecular structures of the other compounds are given in the Supporting Information (Figures S1−S11). Selected bond parameters of **2**−**12** are summarized in Tables 4 and

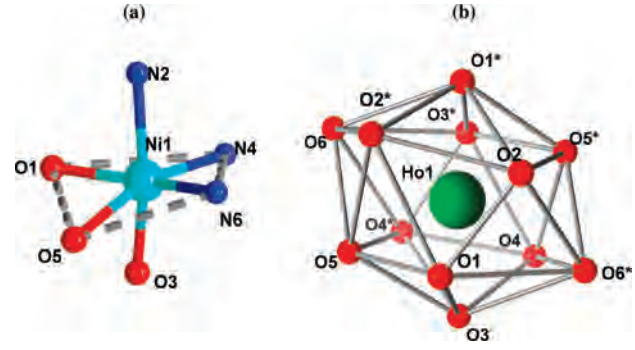

Figure 2. (a) Distorted octahedral environment around the nickel atom in **11**. (b) Distorted icosahedral coordination sphere around the holmium(III) metal ion in **11**.

5. The heterobimetallic trinuclear cation is formed as a result of the coordination action of two completely deprotonated ligands, $[L]^{3-}$. Each L^{3-} encapsulates a Ni^{2+} by a facial coordination involving three imino nitrogen atoms and three phenolate oxygen atoms. Two in situ formed metallo-ligands $[LNi]^-$ bind to a central lanthanide ion generating the

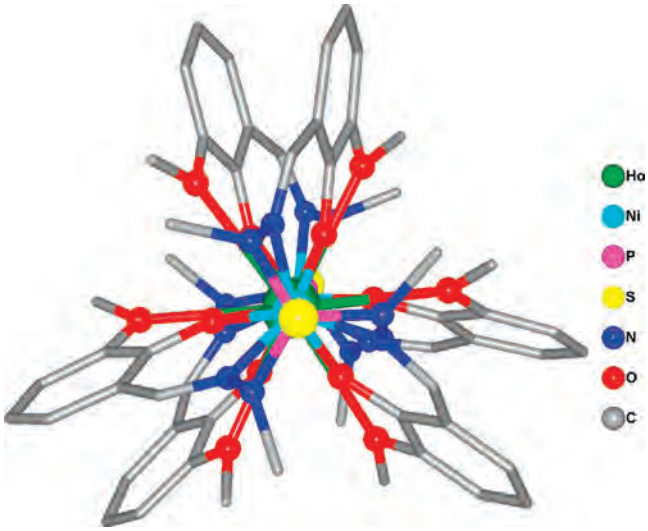

Figure 3. Paddle-wheel arrangement of ligands around the metal centers when viewed along the linear intermetal axis in **11**.

$[LNi-Ln-NiL]^+$ core (parts a and b of Figure 1). As shown in part c of Figure 1, phenolate oxygen atoms function as bridging ligands between the 3d and 4f metal ions.

The coordination environment around the nickel site is distorted octahedral (3N, 3O) (part a of Figure 2), whereas for the lanthanide ion, distorted icosahedral (12O) geometry is observed (part b of Figure 2). Thus, an inversion center is located on the central lanthanide metal ion that is surrounded by an all-oxygen coordination environment: six oxygens being of phenolic nature and the six others originating from −OMe groups. The overall disposition of the ligand framework around the three metal ions gives a paddle-wheel type configuration when the molecule is viewed along the linear Ni−Ln−Ni arrangement (Figure 3). The linearity of the heterometallic assembly is reflected in the Ni−Ln−Ni bond angles found in **2**−**12** (Table S1 in the Supporting Information).

An inspection of Tables 4 and 5 reveals that the $Ni-O_{avg}$and $Ni-N_{avg}$ bond distances for all of the complexes are very similar and range from 2.056 to 2.063 Å for Ni−O and from 2.058 to 2.067 Å for Ni−N bonds. These distances are longer than those observed for the homometallic trinuclear complexes L'_2Ni_3, where $L'H_3$ is a related ligand (S)P[N(Me)N=CH−C_6H_4-*2*-OH]$_3$ without the −OMe groups present in LH_3.[21] It is worth noting the bond distance data of **2**−**12** given in Tables 4 and 5 reflect the lanthanide contraction as illustrated in Figure 4. The $Ln-O(phenolate)_{avg}$ bond distances decrease monotonically and follow the lanthanide contraction: La (2.538(3)) > Ce (2.513(4)) > Pr (2.495(4)) > Nd (2.482(4)) > Sm (2.450(5)) > Eu (2.435(4)) > Gd (2.423(4)) > Tb (2.409(4)) > Dy (2.392(3)) > Ho (2.377(4)) > Er (2.361(4)). However, the same trend is not observed for the $Ln-O(methoxy)_{avg}$ distances that do not really change, probably because of the weak coordination of this group to the Ln ions. It is also interesting to note that both the end−end Ni−Ni as well as Ni−Ln distances found in **2**−**12** follow the lanthanide contraction and decrease proceeding from **2** to **12** (Tables 4 and 5).

Magnetic Properties. 2, 6, and 7: Simple Paramagnetic Complexes. At room temperature, the χT products of **2**, **6**, and **7** are 2.3, 2.4, and 3.8 $cm^3 \cdot K/mol$, respectively (Figure 5). These values are in very good agreement with the presence of two $S = 1$ Ni^{II} ions ($S = 1$, $C = 1$ cm^3 K/mol expected for $g = 2$) and one diamagnetic lanthanum(III) ion for **2** (the expected χT value is 2.3 cm^3 K/mol with $g_{Ni} = 2.14$) and one samarium(III) ion ($S = {}^5/_2$, $L = 0$ $^6H_{5/2}$ $C = 0.09$ $m^3 \cdot K/mol$ with $g = {}^2/_7$, leading to an estimated χT value of 2.4 cm^3 K/mol with $g_{Ni} = 2.14$) for **6**.[6] For the analogous europium complex (**7**), the χT product at 300 K is significantly higher than expected for two $S = 1$ Ni^{II} ions and one europium(III) ion ($S = 0$, $^7F_0$) that possesses a diamagnetic ground state. This result is explained by the presence of the first excited states that are sufficiently low in energy to be thermally populated at 300 K. As these thermally populated levels are much more magnetic than the ground state, the experimental χT product (3.8 $cm^3 \cdot K/mol$) is higher than estimated.[23] As shown in Figure 5, lowering the temperature induces a continuous decrease of the χT product of **7** to a value of 2.4 cm^3 K/mol at 9 K. This behavior is the expected result of the progressive and finally total depopulation of the magnetic excited states of the europium(III) metal ions. At lower temperatures, χT further decreases to reach 1.3 cm^3 K/mol at 1.8 K. Similarly, for **2** and **6** below 10 K, the χT product decreases to 1.4 and 1.9 cm^3 K/mol at 1.8 K (inset of Figure 5). Therefore, below ca. 10 K, the three compounds exhibit a very similar ground state, confirming that the europium(III) low-lying excited states are completely depopulated for **7**. Above 10 K, the χT product of **2** and **6** remain quasi-constant, indicating a Curie-type paramagnetism or *in other words* that the spins of the metal ions are almost uncoupled within the trinuclear complex and that no magnetic low lying excited states are thermally populated for these compounds.

To model the magnetic properties of **2** and **6**, in particular in the low-temperature region, two parameters have to be considered, (i) the intramolecular Ni···Ni magnetic interactions, J, (note that the Ni···Sm interaction is going to be negligibly small due to the extremely weak paramagnetism of the samarium(III) center), and (ii) the magnetic anisotropy (D_{Ni}) brought by the $S = 1$ nickel(II) metal ions. Therefore, the complete Hamiltonian should be written as follows: $H = -2JS_{Ni1}S_{Ni2} + 2D_{Ni}S_{Ni,z}{}^2$. Nevertheless, our attempts failed to simulate the χT vs T data with the theoretical susceptibility deduced from this model[24,25] as multiple equivalent solutions have been obtained. Therefore, this model has been simplified

(22) (a) *SMART & SAINT Software Reference manuals, version 6.45*; Bruker Analytical X-ray Systems, Inc.: Madison, WI, 2003. (b) Sheldrick, G. M. *SADABS a software for empirical absorption correction; ver. 2.05* University of Göttingen: Göttingen, Germany, 2002. (c) *SHELXTL Reference Manual, ver. 6.1*; Bruker Analytical X-ray Systems, Inc.: Madison, WI, 2000. (d) Sheldrick, G. M. *SHELXTL ver. 6.12*, Bruker AXS Inc., Madison, WI, 2001. (e) Sheldrick, G. M. *SHELXL97, Program for Crystal Structure Refinement*; University of Göttingen: Göttingen, Germany, 1997. (f) Bradenburg, K. *Diamond, ver. 3.1eM*; Crystal Impact GbR: Bonn, Germany, 2005.

Table 4. Selected Bond Distances (Angstroms) for **2**−**7**

	2	3	4	5	6	7
P−S	1.925(2)	1.9241(17)	1.9237(16)	1.9243(19)	1.923(2)	1.9251(17)
P−Navg	1.6587(7)	1.657(6)	1.663(5)	1.660(6)	1.6663(6)	1.661(5)
N−N	1.459(7)	1.446(6)	1.448(5)	1.445(7)	1.460(8)	1.445(6)
	1.453(7)	1.452(6)	1.465(6)	1.446(6)	1.434(7)	1.440(7)
	1.459(7)	1.465(6)	1.454(6)	1.457(7)	1.448(8)	1.463(6)
N═C	1.282(10)	1.282(7)	1.292(7)	1.277(8)	1.273(9)	1.296(7)
	1.277(10)	1.283(7)	1.290(7)	1.282(8)	1.279(9)	1.291(7)
	1.274910)	1.286(7)	1.293(7)	1.267(8)	1.267(9)	1.266(7)
Ni−N	2.054(5)	2.055(5)	2.060(4)	2.059(3)	2.055(5)	2.055(4)
	2.057(5)	2.058(4)	2.061(4)	2.062(5)	2.062(5)	2.065(4)
	2.063(6)	2.065(5)	2.073(4)	2.068(5)	2.076(5)	2.067(4)
	2.058(6)[a]	2.059(5)[a]	2.065(4)[a]	2.063(5)[a]	2.064(5)[a]	2.062(4)[a]
Ni−O	2.056(5)	2.049(4)	2.045(4)	2.049(4)	2.057(5)	2.048(4)
	2.059(5)	2.063(4)	2.066(4)	2.063(4)	2.062(5)	2.060(4)
	2.068(4)	2.065(3)	2.069(3)	2.069(3)	2.064(3)	2.069(3)
	2.061(5)[a]	2.059(4)[a]	2.060(4)[a]	2.060(4)[a]	2.061(5)[a]	2.059(4)[a]
Ln−$O_{phenolate}$	2.533(5)	2.504(4)	2.488(4)	2.475(4)	2.442(5)	2.432(4)
	2.541(5)2	0.515(3)	2.497(3)	2.481(3)	2.451(3)	2.434(3)
	2.541(3)	2.520(4)	2.501(4)	2.490(4)	2.458(5)	2.439(4)
	2.538(5)	[a]2.513(4)[a]	2.495(4)[a]	2.482(4)[a]	2.450(5)[a]	2.435(4)[a]
Ln−O_{OMe}	2.884(5)	2.882(4)	2.878(4)	2.885(4)	2.904(5)	2.886(4)
	2.904(4)	2.906(4)	2.882(4)	2.907(4)	2.932(5)	2.919(3)
	2.908(6)	2.908(3)	2.901(3)	2.911(3)	2.935(4)	2.923(4)
	2.8987(6)[a]	2.8987(4)[a]	2.887(4)[a]	2.901(4)[a]	2.9237(5)[a]	2.9093(4)[a]
Ni−Ni	6.8409(11)	6.7942(9)	6.7617(16)	6.7337(10)	6.6679(11)	6.6449(9)
Ni−Ln	3.4209(7)	3.3973(5)	3.3811(9)	3.3673(7)	3.3345(7)	3.3230(6)

[a] Average bond distances.

Table 5. Selected Bond Distances (Angstroms) for **8**−**12**

	8	**9**	**10**	**11**	**12**
P−S	1.9239(18)	1.9259(18)	1.9257(15)	1.9249(16)	1.9265(17)
P−Navg	1.665(5)	1.664(5)	1.665(4)	1.666(6)	1.665(6)
N−N	1.447(6)	1.454(6)	1.450(6)	1.460(5)	1.458(6)
	1.459(7)	1.455(6)	1.440(5)	1.444(5)	1.452(6)
	1.458(8)	1.450(7)	1.460(6)	1.453(6)	1.457(5)
N═C	1.286(7)	1.281(8)	1.284(6)	1.280(6)	1.295(7)
	1.273(7)	1.273(8)	1.290(6)	1.296(6)	1.290(6)
	1.286(7)	1.291(8)	1.282(6)	1.265(7)	1.291(6)
Ni−N	2.059(4)	2.060(4)	2.051(4)	2.048(4)	2.049(4)
	2.063(4)	2.070(4)	2.068(4)	2.054(4)	2.054(4)
	2.073(5)	2.071(5)	2.069(4)	2.065(4)	2.071(4)
	2.065(5)[a]	2.067(5)[a]	2.063(4)[a]	2.056(4)[a]	2.058(4)[a]
Ni−O	2.043(4)	2.046(4)	2.042(4)	2.052(4)	2.048(4)
	2.067(3)	2.057(4)	2.068(3)	2.058(4)	2.070(4)
	2.066(4)	2.066(3)	2.070(4)	2.067(3)	2.070(3)
	2.059(4)[a]	2.056(4)[a]	2.060(4)[a]	2.059(4)[a]	2.063(4)[a]
Ln−$O_{phenolate}$	2.421(4)	2.407(4)	2.389(3)	2.369(4)	2.358(4)
	2.422(4)	2.408(4)	2.393(4)	2.378(3)	2.360(3)
	2.426(3)	2.412(3)	2.393(3)	2.383(4)	2.366(4)
	2.423(4)[a]	2.409(4)[a]	2.392(4)[a]	2.377(4)[a]	2.361(4)[a]
Ln−O_{OMe}	2.877(4)	2.872(4)	2.873(3)	2.884(4)	2.873(4)
	2.901(4)	2.920(4)	2.929(2)	2.9575(4)	2.9528(4)
	2.909(3)	2.924(3)	2.948(2)	2.9770(4)	2.9879(4)
	2.8957(4)[a]	2.905(4)[a]	2.917(3)[a]	2.939(4)[a]	2.938(4)[a]
Ni−Ni	6.6268(19)	6.5952(9)	6.5570(8)	6.5056(10)	6.4845(8)
Ni−Ln	3.3142(10)	3.2976(6)	3.2795(5)	3.254(6)	3.2440(6)

[a] Average bond distances.

to avoid over-parametrization, considering: (i) $J = 0$[26] and (ii) $D_{Ni} = 0$.[27] Both models lead to identical quality of data/theory agreement, as shown Figure 5 with $g = 2.15(5)$ and $J/k_B = -0.45(5)$ K or $D_{Ni}/k_B = -9.2(5)$ K for **2** and with $g = 2.20(5)$ and $J/k_B = -0.25(5)$ K or $D_{Ni}/k_B = -5.4(5)$ K for **6**. Even if large D_{Ni} have been reported for nickel(II) metal ions,[28,29] it is likely that the deduced D_{Ni} values are really too large for these type of complexes. Therefore, this result strongly suggests that antiferromagnetic intramolecular Ni···Ni interactions (Figure S11 in the Supporting Information) are present in these compounds and are partially or totally responsible for the decrease of χT product at low temperatures. This hypothesis is confirmed by the magnetic properties of **8** (vide infra), indicating that the anisotropy

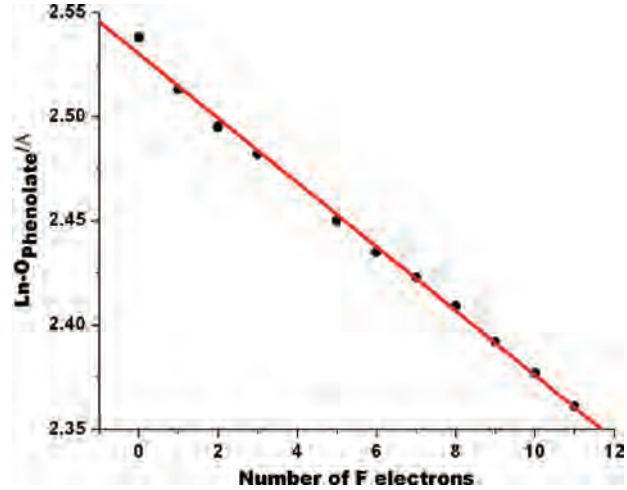

Figure 4. Ln−$O_{phenolate}$ distance following the lanthanide contraction.

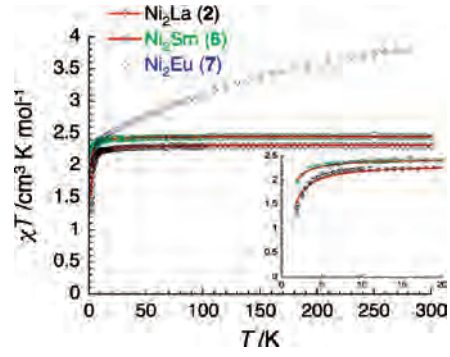

Figure 5. Temperature dependence of the χT product at 1000 Oe for **2**, **6**, and **7** (with $\chi = M/H$ normalized per mol); inset: expansion view of the χT vs T plot at low temperatures. Solid lines show the best fits obtained the magnetic models described in the text.

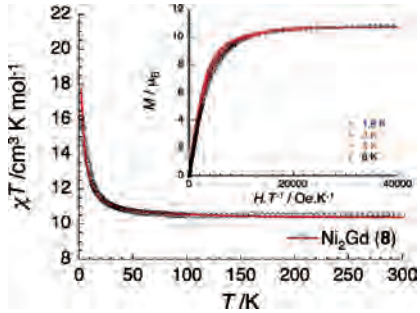

Figure 6. Temperature dependence of the χT product at 1000 Oe for **8** (with $\chi = M/H$ normalized per mol); inset: M vs H/T plot at low temperatures. Solid lines show the best fits obtained the magnetic models described in the text.

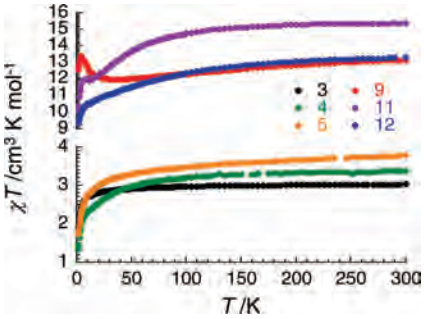

Figure 7. Temperature dependence of the χT product at 1000 Oe for **3**, **4**, **5**, **9**, **11**, and **12** (with $\chi = M/H$ normalized per mol).

introduced by the nickel(II) metal ions is negligible. Thus, the model with $D_{Ni} = 0$ is certainly the more physically acceptable to describe the magnetic properties of these complexes. Nevertheless, it is worth adding that the given values of J should be taken with caution as even the presence of a very weak anisotropy can enhance artificially its estimation.

Trinuclear Ni−Gd−Ni $S_T = {}^{11}/_2$ (8). At room temperature, the χT product of **8** is 10.5 cm^3 K/mol, in very good agreement with the presence of one Gd^{III} ion ($S = {}^7/_2$, $C =$ 7.875 cm^3 K/mol with $g = 2$)[6] and two $S = 1$ nickel(II) ions. Decreasing the temperature, the χT product at 1000 Oe continuously increases to reach 15.9 cm^3 K/mol at 1.8 K, indicating dominant ferromagnetic Ni···Gd interactions within the trinuclear complex. Application of the van Vleck equation[30] to the Kambe's vector coupling scheme[31] allows one to determine an analytical expression of the magnetic susceptibility from the following spin Hamiltonian: $H = -2J(S_{Ni1}S_{Gd} + S_{Gd}S_{Ni2})$, where S_i the spin operators with $S = 1$ and $S = {}^7/_2$ for the nickel(III) and gadolinium(III) metal ions respectively, and J is the Ni···Gd magnetic interaction (it is worth noting that there is only one Ni···Gd interaction by symmetry as shown by the X-ray structural analysis). So, the susceptibility in the low-field limit can be expressed as:

$$\chi = \frac{Ng^2\mu_B^2}{2k_BT} \times \frac{(10 + 35(A) + 84(B) + 165(C) + 286 \exp(32J/k_BT))}{(4 + 6(A) + 8(B) + 10(C) + 12 \exp(32J/k_BT))}$$

with $A = \exp(5J/k_BT) + \exp(9J/k_BT)$, $B = \exp(12J/k_BT) + \exp(16J/k_BT) + \exp(18J/k_BT)$, and $C = \exp(21J/k_BT) + \exp(25J/k_BT)$.[19d] The best set of parameters obtained using this Heisenberg model is $J/k_B = +0.54(3)$ K and $g = 2.04$ (Figure 6). The sign of the magnetic interaction implies that this [Ni_2Gd] complex possesses an $S_T = {}^{11}/_2$ spin ground state that is not solely populated at 1.8 K as the χT product does not saturate to the $S_T = {}^{11}/_2$ expected value of 17.875 cm^3 K/mol.

At low temperatures, the magnetization measurements done as a function of the field reveal a saturation under 7 T at 10.8 μ_B, in good agreement with the theoretical value for an $S_T = {}^{11}/_2$ spin ground state. Nevertheless, as shown in the inset of Figure 6, the $S = {}^{11}/_2$ Brillouin function is not reproducing perfectly the experimental data at 1.8 K (with $g = 1.96(10)$), supporting the presence of thermally populated excited states even at this temperature. It is also interesting to mention that the relatively rapid saturation of the magnetization at high fields indicates the absence of a marked magnetic anisotropy that is also confirmed by the M versus H/T data that are roughly all superposed on a single master-curve as expected for isotropic systems. Whereas gadolinium(III) is usually a magnetically isotropic metal ion, this observation indicates that the magnetic anisotropy induced by the presence of the nickel(II) ions in these series of compounds is also quite small.

Trinuclear Ni−Ln−Ni Compounds: 3, 4, 5, 9, 11, and 12. At room temperature, the χT products of **3**, **4**, **5**, **9**, **11**, and **12** are 3.0, 3.4, 3.7, 13.2, 15.4, and 13.4 cm^3 K/mol, respectively (Figure 7). These values are globally in very good agreement with the presence of two $S = 1$ nickel(II) ions ($S = 1$, $C = 1$ cm^3 K/mol with $g = 2$) and one trivalent lanthanide ion (the expected χT values are 2.8, 3.6, 3.6, 13.8, 16.1, and 13.5 cm^3 K/mol for the cerium, praseodymium, neodymium, terbium, holmium, and erbium complexes).[6]

When the temperature is lowered, the χT product at 1000 Oe for **3**, **4**, **5**, **11**, and **12**, decreases to a minimum value at 1.8 K of 1.85, 1.3, 1.7, 10.0, and 9.3 cm^3 K/mol, respectively. Because of the presence of lanthanide ions, the temperature dependence of the magnetic susceptibility and thus the observed decrease of the χT product are mainly governed by the thermal depopulation of the ground-state sublevels that result from spin−orbit coupling and a low symmetry crystal field.[32] Moreover, as the 4f electrons are shielded by the occupied outer shells of 5s and 5p electrons, the 4f

(23) Caneschi, A.; Dei, A.; Gatteschi, D.; Poussereau, S.; Sorace, L *Dalton Trans.* **2004**, 1048.
(24) Borras-Almenar, J. J.; Clemente-Juan, J. M.; Coronado, E.; Tsukerblat, B. S. *Inorg. Chem.* **1999**, *38*, 6081.
(25) Borras-Almenar, J. J.; Clemente-Juan, J. M.; Coronado, E.; Tsukerblat, B. S. *J. Comput. Chem.* **2001**, *22*, 985.
(26) Boca, R. *Coord. Chem. Rev.* **2004**, *248*, 757.
(27) O'Connor, C. J. *Prog. Inorg. Chem.* **1982**, *29*, 203.
(28) Charron, G.; Bellot, F.; Cisnetti, F.; Pelosi, G.; Rebilly, J. N.; Rivière, E.; Barra, A. L.; Mallah, T.; Policar, C. *Chem.—Eur. J.* **2007**, *13*, 2774.
(29) Rogez, G.; Rebilly, J. N.; Barra, A. L.; Sorace, L.; Blodin, G.; Kirchner, N.; Duran, M.; van Slageren, J.; Parsons, S.; Ricard, L.; Marvilliers, A.; Mallah, T *Angew. Chem., Int. Ed.* **2005**, *44*, 1876.
(30) van Vleck, J. H. *The Theory of Electric and Magnetic Susceptibiilty*; Oxford University Press: Oxford, 1932.
(31) Kambe, K. *J. Phys. Soc. Jpn.* **1950**, *5*, 48.
(32) Carlin, R. L. *Magnetochemistry*, Springer-Verlag Berlin: Heidelberg, Germany, 1986.

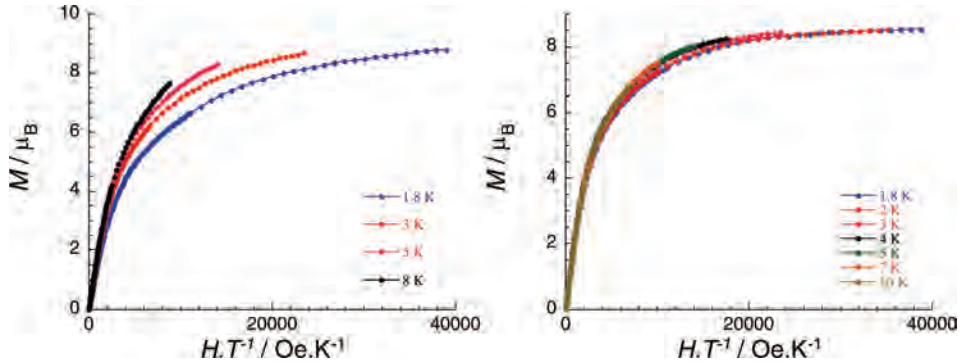

Figure 8. *M* vs *H*/*T* data for **11** (left, similar behavior is observed for **3**, **4**, **5**, and **12**) and **9** (right).

electrons are little involved with the chemical bonding, inducing very weak superexchange and magnetic couplings mainly dominated by dipole−dipole interactions.[32] The magnetic interactions between lanthanide and 3d metal ions are weak in most of the cases. Hence, it is very difficult to determine the relative contributions of the magnetic intramolecular interactions versus thermal depopulation of the Stark levels[32] and whether the evidently weak intramolecular exchange interactions are ferro- or antiferromagnetic.

As exemplified in Figure 8 (left part) for **11**, the low-temperature magnetization measurements as a function of the field reveal a very similar behavior for **3**, **4**, **5**, **11**, and **12**: (i) a slow increase of the magnetization at low field and (ii) a very slow saturation of the magnetization that is not completely achieved at 1.8 K under 7 T. The magnetization values under 7 T and at 1.8 K are 5.2, 4.0, 5.0, 8.8, and 9.9 μ_B respectively. The slow saturation of the magnetization suggests the possible presence of a magnetic anisotropy and/or more likely the presence of low-lying excited states expected with the weak Ni···Ln magnetic interactions already discussed above.

The thermal behavior of **9** is different, with a slight decrease of the χT product between 300 and 30 K to reach 12 cm^3 K/mol. This feature is possibly the result of intramolecular antiferromagnetic interactions and/or more likely the thermal depopulation of the terbium(III) excited states (Stark sublevels of the $^7F_6$ state).[32] Between 30 and 3 K, the χT product increases to reach 13.4 cm^3 K/mol and then below 3 K decreases again to 12.5 cm^3 K/mol at 1.8 K. If the latter variation is probably associated with the presence of magnetic anisotropy or weak antiferromagnetic interaction between trinuclear complexes (as observed in **2**, **6**, and **7**), the increase of the χT product between 30 and 3 K suggests the presence of a high-spin ground-state for this complex that could be the result of either a ferri- or ferromagnetic arrangement of the Ni(II)−Tb(III)−Ni(II) spins.

As shown in Figure 8 (right part), the *M* versus *H* measurements for **9** between 1.8 to 10 K reveal (i) a relative rapid increase of the magnetization at low field (in comparison to the other complexes described in this part), (ii) a rapid saturation of the magnetization that is achieved above 5 T at 1.8 K, and (iii) a value of 8.6 μ_B at 7 T and 1.8 K. This behavior suggests the absence of significant magnetic anisotropy in this system and also a well-defined ground-state that is stabilized by sufficiently large Ni···Tb magnetic interactions. This conclusion is further supported by a *M* versus *H*/*T* plot (Figure 8, right) because the data are almost all superposed on a single master-curve as expected for isotropic systems with a well-defined ground state.

It is worth noting at the end of this paragraph that at the lowest temperature available, namely 1.8 K, no significant hysteresis effect or slow relaxation of the magnetization have been observed for all of these complexes on the *M* versus *H* plot or by the ac technique.

Single-Molecule Magnet Behavior in 10. At room temperature, the measured χT product for **10** is 16.7 cm^3 K/mol as expected at high temperatures in presence of one dysprosium(III) ($S = {}^5/_2$, $L = 5$, $^6H_{15/2}$ $g = {}^4/_3$: $C = 14.17$ cm^3 K/mol)[6] and two $S = 1$ nickel(II) ions. Decreasing the temperature, the χT product at 1000 Oe is first stable and then very slightly decreases to reach 16.0 cm^3 K/mol at 25 K as probably the result of mainly the thermal depopulation of the dysprosium(III) excited states (Stark sublevels of the $^6H_{15/2}$ state).[32] Between 25 and 5 K, the χT product increases to reach 17.6 cm^3 K/mol before a final drop off below 5 K that is probably in relation with the magnetic anisotropy or weak antiferromagnetic interactions between trinuclear complexes (as already observed in **2**, **6**, **7**, and **9**). On the other hand, the increase of the χT product between 25 and 5 K is likely associated with the stabilization of a high-spin ground-state for this complex. As observed for **9**, this large ground state could be the result of either ferri- or ferromagnetic arrangement of the Ni(II)−Dy(III)−Ni(II) spins.

The *M* versus *H*/*T* measurements performed between 1.8 and 10 K reveal (i) a relative rapid increase in the magnetization at low field in accord with a high-spin state for this complex and (ii) a slow saturation of the magnetization that is almost complete at 1.8 K under 7 T, reaching a value of 10.2 μ_B. Moreover, it is worth noting that the *M* vs *H*/*T* data are not superposed on a master-curve as expected for isotropic systems with a well-defined ground state. Therefore, as for **3**, **4**, **5**, **11**, and **12**, this behavior suggests the presence of a significant anisotropy and/or low lying excited states (already suspected from the χT vs *T* data) that prevent the saturation of the magnetization for **10**.

Although at the lowest temperature available (1.8 K), the *M* versus *H* data do not show any sign of significant hysteresis effect (i.e., slow relaxation of the magnetization at the time scale of the dc measurements), ac susceptibility

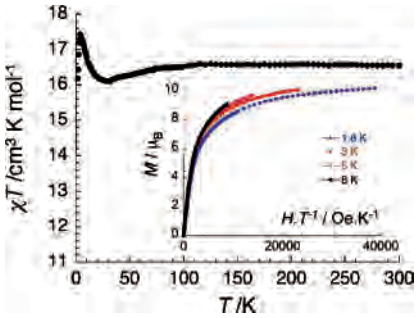

Figure 9. Temperature dependence of the χT product at 1000 Oe for **10** (with $\chi = M/H$ normalized per mol). Inset: M vs H/T data for **10**.

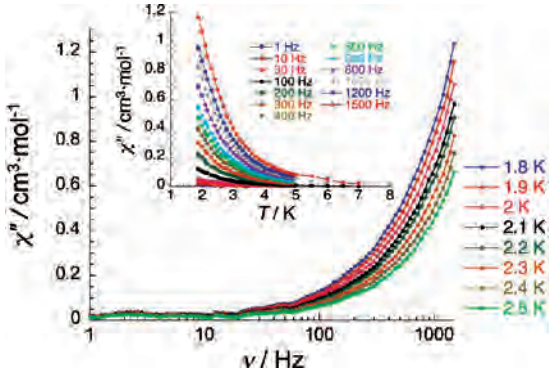

Figure 10. Temperature (inset) and frequency dependence of the out-of-phase ac susceptibility at different frequencies and different temperatures under zero dc field for **10**.

as a function of the temperature at different frequencies and also as a function of the frequency at different temperatures have been performed (Figure 10).

This set of data, shown in Figure 10, demonstrates that **10** exhibits slow relaxation of the magnetization and strongly suggests single-molecule magnet (SMM) properties. SMMs exhibit magnetization slow relaxation induced by a combined effect of their uniaxial anisotropy ($D < 0$) and high-spin ground state (S_T). These two characteristics create a first regime of relaxation that is purely thermally induced by an energy barrier (Δ), equal to $|D|S_T^2$ for integer spins (and $|D|(S_T^2 - {}^1/_4)$ for half-integer spins), between the two equivalent configurations $m_S = \pm S_T$. Below the so-called blocking temperature (T_B), the thermal energy (k_BT) is not anymore able to overcome the Δ barrier, and the spin is trapped in one of the two equivalent configurations. This molecular property can be detected at the bulk level when a magnetic field is applied, saturating the magnetization below T_B. When this field is switched off, the magnetization slowly relaxes with a characteristic relaxation time (τ) that can be measured as a function of the temperature using the time decay of the magnetization and the frequency dependence of the ac susceptibility. τ follows a thermally activated behavior (Arrhenius law): $\tau(T) = \tau_0 \exp(\Delta/k_BT)$ and hysteresis effects with an applied field are observed at a low enough temperature as a signature of a magnetlike behavior. Lower in temperature, a second type of relaxation is observed that is temperature independent. In the zero field, states with $\pm m_S$ quantum numbers have the same energy and quantum tunneling of the magnetization (QTM) between these pairs of levels is possible. The quantum effects are thus responsible

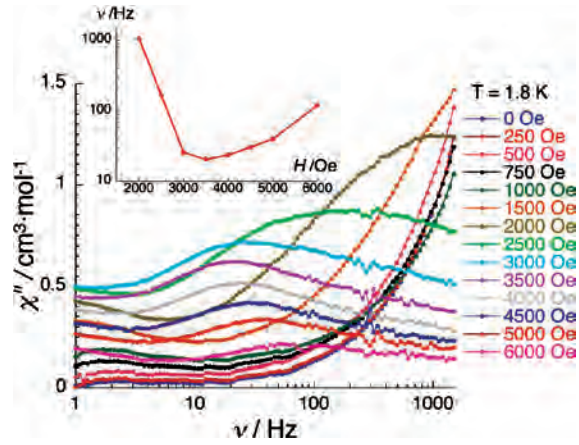

Figure 11. Frequency dependence of the out-of-phase ac susceptibility at different applied dc fields at 1.8 K for **10**. Inset: Field dependence of the characteristic frequency of the magnetization relaxation showing a minimum around 3500 Oe (solid lines are guides for eyes).

for this second relaxation that can be experimentally observed as it becomes faster than the thermally activated relaxation.

Even if the relaxation observed by the ac technique (Figure 10) is clearly temperature dependent, the relaxation time of the magnetization cannot be estimated because the relaxation mode is at a higher frequency than the highest experimentally available frequency (namely 1500 Hz). Nevertheless, at temperatures between the thermal and the quantum regimes, quantum effects are still expected to influence the thermal relaxation. In this intermediate domain of temperature also called the thermally assisted quantum tunneling regime, the energy gap of the Arrhenius law is reduced by the quantum tunneling of the excited states. Δ takes an effective value and thus the observed relaxation time is fastened. Therefore, to study only the thermal relaxation in this regime, a small dc field can be applied to remove the degeneracy of the m_S states, lowering the probability of the zero-field QTM between the $\pm m_S$ states.[7b,10f,16l,33–36] Therefore, applying a small dc field allows, in most of the cases, a good estimation of the energy gap without significantly influencing the pre-exponential factor.[10f,16l,18,33–36]

Hence, the thermal regime of **10** and its characteristic relaxation time above 1.8 K have been further studied, measuring the frequency dependence of the ac susceptibility at 1.8 K and applying small dc fields up to 6000 Oe (Figure 11). As expected, the zero-field quantum tunnelling is reduced by the application of a dc field, and the relaxation time is significantly increased, becoming close to the expected value for the purely thermal regime. While in the zero field, the characteristic frequency is above 1500 Hz at 1.8 K, this frequency decreases with an increasing dc field to reach a minimum value of 20 Hz around 3500 Oe (inset

(33) Wernsdorfer, W. *Adv. Chem. Phys.* **2001**, *118*, 99.
(34) Martínez-Lillo, J.; Armentano, D.; Munno, G. D.; Werndorfer, W.; Julve, M.; Lloret, F.; Faus, J. *J. Am. Chem. Soc.* **2006**, *128*, 14218.
(35) Poneti, G.; Bernot, K.; Bogani, L.; Caneschi, A.; Sessoli, R.; Wernsdorfer, W.; Gatteschi, D. *Chem. Commun.* **2007**, 1807.
(36) (a) Ako, A. M.; Mereacre, V.; Hewitt, E. J.; Clérac, R.; Lecren, L.; Anson, C. E.; Powell, A. K. *J. Mater. Chem.* **2006**, *16*, 2579. (b) Li, D.; Clérac, R.; Wang, G.; Yee, G. T.; Holmes, S. M. *Eur. J. Inorg. Chem.* **2007**, 1341. (c) Kachi-Terajima, C.; Miyasaka, H.; Saitoh, A.; Shirakawa, N.; Yamashita, M.; Clérac, R. *Inorg. Chem.* **2007**, *46*, 5861.

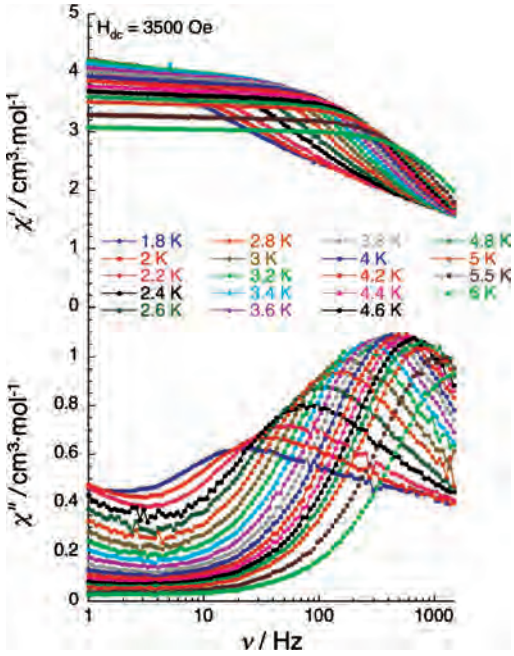

Figure 12. Frequency dependence of the in-phase and out-of-phase ac susceptibility at different temperatures under 3500 Oe applied dc field for **10**.

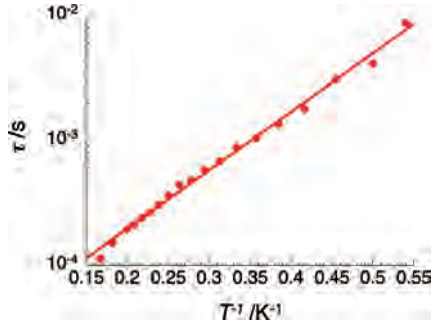

Figure 13. Relaxation time of the magnetization (τ) versus T^{-1} plot under 3500 Oe applied dc field for **10**.

of Figure 11). Therefore, the frequency dependences of the ac susceptibility at different temperatures have been measured at 3500 Oe (Figure 12).

As expected, the slow relaxation of the magnetization is significantly pushed at higher temperatures when 3500 Oe are applied, and the activated behavior of the relaxation time (Figure 13) can be deduced from the measurements shown in Figure 12. The data are perfectly fitted to an Arrhenius law, and the characteristic energy gap, Δ, can be estimated at 10.8 K, whereas the pre-exponential factor, τ_0, amounts to 2.3×10^{-5} s. The energy gap has an experimental value that is comparable to those estimated for similar 3d/4f SMM systems,[15,16,18,35,37] but the pre-exponential factor of the Arrhenius equation is much larger than expected (typical values between 10^{-7} and 10^{-10} s are usually found).[16l] This observation suggests strongly that the quantum pathway of relaxation is only partially suppressed by the applied field of 3500 Oe and hence that the energy gap of the thermally activated relaxation should, in fact, be higher than 10.8 K. Nevertheless, all of the magnetic measurements performed on **10** are consistent with a SMM behavior induced by a large anisotropy brought by the dysprosium(III) metal ion and a high-spin state stabilized by significant intramolecular Ni···Dy interactions.

(37) Mereacre, V.; Ako, A.M.; Clérac, R.; Wernsdorfer, W.; Hewitt, E. J.; Anson, C. E.; Powell, A. K. *Chem. Eur. J.*, 2008; In press.

Concluding remarks

We have designed a multisite coordination ligand LH_3 where three hydrazone arms are anchored on a central phosphorus atom. This ligand containing imino (N), phenolate (O), and methoxy (O) groups as coordination sites effectively mediates the formation of cationic trinuclear $[L_2Ni_2Ln]^+$ complexes. Each of the trinuclear assemblies contains two terminal nickel(II) centers bound in a facial manner by the coordination of three imino and three phenolate oxygen atoms. The residual coordination ability of the phenolate oxygen atoms in conjunction with the oxygen atoms of the −OMe group leads to the encapsulation of the central lanthanide ion whose coordination number is 12. The coordination geometry around the lanthanide metal ion is distorted icosahedral. The perfectly linear arrangement of the three metal ions in the trinuclear array leads to a paddle-wheel-like architecture of the ligands when viewed in the intermetal axis. The Ln−$O_{phenolate}$, Ni−Ni, and Ni−Ln bond distances follow the lanthanide contraction trend. The magnetic properties of these complexes reveal that the lanthanum, cerium, praseodymium, neodymium, samarium, europium, holmium, and erbium analogues are simple paramagnetic systems, whereas the gadolinium-, terbium-, and dysprosium-based complexes possess an high-spin ground-state that is $^{11}/_2$ in the gadolinium case. Moreover, because of the presence of an important magnetic anisotropy brought by the dysprosium(III) ions, the Ni_2Dy complexes exhibit a single-molecule magnet behavior, adding a new member to the small family of 3d/4f SMM systems.

Acknowledgment. We thank the Department of Science and Technology, India, and Council of Scientific and Industrial Research, India, for financial support. V.C. is a Lalit Kapoor Chair Professor of Chemistry. V.C. is thankful for the Department of Science and Technology for a J.C. Bose fellowship. B.M.P. thanks the Council of Scientific and Industrial Research, India, for a Senior Research Fellowship. R.C. thanks Bordeaux 1 University, the CNRS, and the Region Aquitaine for funding.

Supporting Information Available: Diamond pictures of **2**−**10** and **12** and a packing diagram for **6**. This material is available free of charge via the Internet at http://pubs.acs.org.

IC800199X